Korean J. Chem. Eng., 35(7), 1468-1476 (2018)
DOI: 10.1007/s11814-018-0054-4

pISSN: 0256-1115
eISSN: 1975-7220

Interpreting the pH-dependent mechanism of simazine sorption to *Miscanthus* biochar produced at different pyrolysis temperatures for its application to soil

Seoyeon Lee, Junho Han, and Hee-Myong Ro†

Department of Agricultural Biotechnology and Research Institute of Agriculture and Life Sciences, Seoul National University, Seoul 08826, Korea
(*Received 25 January 2018 • accepted 27 March 2018*)

Abstract−Biochar has received considerable attention as an eco-friendly bio-sorbent; however, multifarious characteristics caused by pyrolysis and feedstock pose difficulties in its application. We characterized the pH-dependent sorption of the pesticide simazine on *Miscanthus* biochar produced at two pyrolysis temperatures (400 and 700 °C; hereafter B-400 and B-700). The specific surface-area (SSA) of the micro- and nanopores, elemental composition, surface acidity and infrared spectra were determined. The SSA was greater in B-700 than in B-400, and the former had greater SSA in micro-pores and lower SSA in nanopores than the latter. During pyrolysis, the single-bond structures of the feedstock were converted to aromatic structures, and further pyrolysis led to ligneous structures. Alterations in pore structure and concave-up Scatchard plot corroborated the presence of two sorption mechanisms: electrostatic attractions (S_{es}) and hydrophobic attractions (S_{hp}). Decreases in maximum sorption in the $q_{max\text{-}L}$ with increasing pH was due to decreased S_{es} *via* deprotonation of carboxylic groups on biochar, while those in the $q_{max\text{-}H}$ with increasing pyrolysis temperature were due to decreased S_{hp}, resulting from pore structure deformation. We believe that our approach, which addresses the pH-dependence of charge density of sorbate and sorbent, could contribute to a better understanding of the behavior of simazine.

Keywords: Simazine, *Miscanthus* Biochar, Pyrolysis Temperature, pH-dependent Sorption, Scatchard Plot

INTRODUCTION

Biochar, which is a carbon-rich material produced through pyrolysis of various feedstocks under diverse circumstances [1], has received increased attention because of its applications to wastewater treatment, global warming mitigation, soil fertility improvement, pollution remediation, agricultural waste recycling and carbon sequestration [2-4]. Many attempts have been made to study biochar application; however, unexpected or inconsistent results have frequently occurred in *in situ* application, while laboratory experiments have shown great potential [5,6]. Main causes of discrepancies arise from complex characteristics and a lack of understanding of the fundamental mechanism [7,8].

Recent studies showed that feedstock and pyrolysis predominantly determine biochar characteristics [9,10]. Of various pyrolysis parameters, pyrolysis temperature (PT) is a key factor that governs the characteristics of biochar [8], because thermal decomposition of specific molecular structures needs specific temperatures [11,12]. Previous studies revealed that the cation exchange capacity, pH and surface area of biochar alters dramatically around 500 °C [10,13,14]. Therefore, thermal decomposition determines not only pore-geometry and specific surface-area (SSA) but also distinctive hydrophobic and hydrophilic surfaces [15-17].

Structural and chemical transformations during pyrolysis render biochar a promising biosorbent for inorganic/organic pollutants. High sorption capacity of biochar is due to the presence of oxygenated functional groups and inorganic residue fractions for inorganic pollutants [18-21] and associated with aromatic composition of its porous structures for organic pollutants [22,23]. Since the nature of the surface charge is due to the presence of acidic/basic functional groups in biochar, it is a function of solution-pH and point-of-zero net charge (PZNC) of the sorbent [24]. Therefore, knowledge of pH-dependent sorption is a prerequisite to understanding the sorption mechanism for inorganic/organic pollutants [25,26]. Despite extensive investigations, the mechanisms responsible for the effect of solution-pH on the sorption of sorbates to sorbents are not well-understood due to their heterogeneity.

Changes in acidic functional groups on the surface of activated carbons can lead to significant changes in the sorption mechanisms for organic pollutants [25,27]. Therefore, acidic and basic functional groups present on biochar surface play a central role by attracting charged ions [20] or repelling hydrophobic organic pollutants [28]. Since oxygen-containing carboxylic, lactonic, and phenolic functional groups are particularly responsible for sorption behavior of biochar [29], knowledge of the effects of changes in these functional groups on sorption mechanisms will contribute to understanding of the interaction of organic pollutants with various types of biochar.

Simazine [2-chloro-4,6-bis(ethylamino)-s-triazine] is a herbicide that has lone-pair electrons in its structure. Recent evidence suggests that simazine poses a threat to ground and surface water quality [30,31] due to its low solubility in water and comparative

†To whom correspondence should be addressed.
E-mail: hmro@snu.ac.kr

nonvolatility [32]. Under acidic pH conditions below the negative logarithmic acid dissociation constant (pK_a), simazine is positively charged due to protonation. Otherwise, it behaves as a neutral organic pollutant under the pH above pK_a [33,34]. When the pH is lower than PZNC, the sorbent surface is positively charged and the degree of protonation decreases with increasing pH; otherwise, the surface is negatively charged [35]. Therefore, the behavior of simazine across the environmental pH range is necessary to study mechanistic simazine sorption to the surface of a sorbent that has a certain PZNC.

Sorption mechanisms between inorganic sorbates and metal-based sorbent can be determined using X-ray- and electron-based methods [36,37]; however, these methods are not applicable to sorption between organic pollutants and organic sorbents because organic pollutants are easily decomposed under the radiation of X-rays and electrons [38]. As alternatives, several theoretical isotherms have been employed to interpret the sorption mechanisms: Langmuir, Freundlich and Dubinin-Radushkevich isotherms. Particularly, the Dubinin-Radushkevich isotherm can formulate adsorption following a pore-filling mechanism to predict sorption at homogeneous and heterogeneous surfaces [39]. Therefore, comparison of the fitting results obtained from sorption isotherms can enable prediction of sorption mechanisms of an organic sorbate onto the homogeneous or heterogeneous surface of the sorbent.

Our objectives were to identify differences in the physicochemical characteristics of *Miscanthus* biochar produced at two different PTs, predict the behavior of simazine in the environment, interpret the pH-dependent mechanism of simazine sorption to biochar using three isotherm models and Scatchard plot analysis, and present a comprehensive approach to assessing and predicting the fate and behavior of simazine.

MATERIALS AND METHODS

1. Physicochemical Characteristics of Biochar

Two types of biochar were produced from a *Miscanthus* feedstock at different PTs (400 and 700 °C) (hereafter, B-400 and B-700), which is lower or higher than 500 °C [10,13,14]. The rate of heating was approximately 10 °C min^{-1}, and the target temperatures were maintained for 1 h for the completion of pyrolysis under N_2 gas purging. Biochar was ball-milled (MM400, Retsch, Germany), and sieved through a 106-μm mesh to minimize size-effects [40]. We performed size fractionation using Analysette 3 pro (Fritsch, Germany) to identify the fractions of <25 μm, 25-53 μm and 53-106 μm, respectively. The SSA of biochar was determined using the Brunauer-Emmett-Teller isotherm with two gas adsorbates: N_2 (ASAP 2010, Micromeritics, USA) for nanopores (<1.5 nm) and CO_2 (BELSORP-mini II, Microtrac BEL, Japan) for both nano- and micropores (>1.5 nm) [9,41]. The PZNC was determined using the pH drift method [35].

Carbon (C), hydrogen (H), nitrogen (N), and sulfur (S) were analyzed using an elemental analyzer (Flash 2000, Thermo, USA). Oxygen (O) was calculated by subtracting each percent of C, H, N and S from 100% [10]. Acidic functional groups of biochar were determined by Boehm's titration [42,43]. Biochar was pretreated with dilute HCl (pH 2) to minimize side-effects [44], and then added to each 20 mL of three bases of 0.05 M solutions ($NaHCO_3$, Na_2CO_3, and NaOH) on a flask-shaker at 160 rpm for 24 h. Each mix was centrifuged using an MF-600 centrifuge (Hanil, Korea) at 4,000 rpm for 40 min. Ten milliliters of each supernatant was back-titrated with 0.01 M HCl using an automatic titrator (702 SM Titrino, Metrohm, Switzerland). Yield content was calculated by dividing the weight of biochar after pyrolysis by the weight of biochar feedstock before pyrolysis, and ash content was determined after the combustion of the samples at 750 °C [45,46].

Fourier-transform infrared (FT-IR) spectra of biomass and its derived biochar were obtained using an IR Tracer-100 FT-IR spectrometer (Shimadzu, Japan) equipped with a MIRacle attenuated total reflectance (ATR) accessory (Piketech, USA) with a ZnSe crystal plate at an incidence angle of 45° [11]. The resolution was set to 4 cm^{-1}, and the spectral range covered the 4,000-650 cm^{-1}. Sixty-four scans were collected for each measurement, and ATR correction and smoothing were applied to minimize the difference in penetration depth. Concentration of inorganic elements was measured by X-ray fluorescence (XRF) spectrometer (S4 Pioneer, Bruker, USA) with power settings of 4 kW under a helium purge. Apparent density of biochar was measured following the ASTM D-285 procedure.

2. Batch Sorption Experiments

We conducted four batch experiments: sorption kinetics (Method S1), degradation kinetics (Method S2), speciation (Method S3), and sorption isotherms (Methods S4 and S5). All reagents were purchased from Sigma-Aldrich (USA), and concentrations of simazine and $CaCl_2$ were 5 mg L^{-1} (maximum solubility) and 0.05 M, respectively [40]. The pH was adjusted daily with 0.1 M HCl or 0.1 M NaOH for degradation kinetics, and with 1 M HCl or 1 M NaOH for sorption isotherms. Each sample was allowed to equilibrate in a 30 mL amber glass vial with a Teflon-lined cap on a vial-shaker at 160 rpm for 81 h under controlled room temperature (25 °C) conditions, and each mix was filtered through a 0.45-μm nylon membrane filter. For sample extraction, 2 mL of hexane was injected into 10 mL of each filtrate. One milliliter of supernatant was transferred into a 2 mL amber vial with a rubber cap for GC analysis (Method S6). All experiments were performed in triplicate.

3. Data Analysis and Fitting

A formulation that simulates simazine speciation was proposed based on the Henderson-Hasselbalch equation (Eq. (1)) [47], with the pKa of simazine (1.7) [47].

$$pH = pKa + \log([S]/[HS^+]) \quad (1)$$

where [S] and $[HS^+]$ are the concentrations of neutral and protonated simazine (mol L^{-1}), respectively. Concentration of simazine sorbed (q_{eq}, mg kg^{-1}) was calculated from differences between the initial and equilibrium concentrations in solution (Eq. (2)):

$$q_{eq} = \frac{(C_0 - C_{eq}) \times V}{m} \quad (2)$$

where C_0 and C_{eq} are the initial and equilibrium concentrations of simazine (mg L^{-1}) in solution, and m (kg) and V (L) are the mass of sorbent and volume of solution, respectively.

Percent simazine recovery (Eq. (3)) was obtained by extracting

the sorbed simazine using methanol [48], and 98-103% (data excluded).

$$\text{Recovery} = \frac{(C_{eq} + C_{ex})}{C_0} \times 100 \quad (3)$$

where C_{ex} is the concentration (mg L^{-1}) after methanol-extracted.

A first-order kinetics (Eq. (4)) was applied to describe the degradation of simazine [49].

$$\ln C_t = \ln C_0 - k_{dg} \cdot t \quad (4)$$

where C_t is the concentration (mg L^{-1}) at time t (h) and k_{dg} is the rate constant (mg $L^{-1}h^{-1}$) at 1/t. Isotherm results at pH values (3, 6 and 9) were fitted to the Langmuir, Freundlich, and Dubinin-Radushkevich isotherm [39,50].

The Langmuir model is expressed as follows:

$$q_{eq} = \frac{q_{max} \cdot K_L \cdot C_{eq}}{(1 + K_L \cdot C_{eq})} \quad (5)$$

where K_L is a constant (L mg^{-1}) related to energy, and q_{max} is the maximum sorption capacity (mg kg^{-1}).

The Freundlich model is expressed as follows:

$$q_{eq} = K_F \cdot C_{eq}^{1/n} \quad (6)$$

where K_F (mg kg^{-1}(mg L^{-1})$^{-n}$) and 1/n are the equilibrium constants indicative of the sorption capacity and intensity, respectively.

The Dubinin-Radushkevich model, which describes non-ideal adsorption by heterogeneous surface energies, is expressed as follows [51]:

$$q_{eq} = q_{max} \cdot e^{(-\beta \cdot F^2)} \quad (7)$$

$$F = R \cdot T \cdot \ln\left(1 + \frac{1}{C_{eq}}\right) \quad (8)$$

where β is related to mean sorption energy (mol^2 kJ^{-2}), F is the Polanyi potential, R is the gas law constant (kJ mg^{-1} K^{-1}), and T is absolute temperature (K). This model serves as a proxy to check whether sorption follows physisorption or chemisorption. The E_s indicates the free energy changes (kJ mol^{-1}) when one mole of ions is transferred into infinite space from its sorbent space during sorption, serving as a criterion to distinguish between physisorption and chemisorption (Eq. (9)).

$$E_s = \frac{1}{\sqrt{2 \cdot \beta}} \quad (9)$$

To compare the applicability of the model, the percent normalized standard deviation (Δq) was calculated as follows [52]:

$$\Delta q = 100 \times \sqrt{\frac{\sum_{i=1}^{n}\left[\left(\frac{q_{exp} - q_{cal}}{q_{exp}}\right)_i\right]^2}{n-1}} \quad (10)$$

where q_{exp} and q_{cal} are measured and calculated amount of simazine sorbed on biochar (mg kg^{-1}) for the number of experimental points (n).

Scatchard plot (Eq. (11)) is used to evaluate the affinities of binding sites for a particular sorption [53,54].

$$\frac{q_{eq}}{C_{eq}} = -\left(\frac{1}{K_{ds}}\right) q_{eq} + \frac{q_{max}}{K_{ds}} \quad (11)$$

where K_{ds} is the dissociation constant (mg L^{-1}) of the binding site. Lower K_{ds} indicates involvement of more active sites for sorption [53]. A plot that deviates from linearity means the presence of more than one type of binding site, while a linear plot assumes that the binding sites are identical and independent [39,55].

RESULTS AND DISCUSSION

1. Physiochemical Characteristics of Biochar

The SSA was estimated at 5.6 m^2 g^{-1} for micro-pores and 191.6 m^2 g^{-1} for nanopores in B-400, and 236.3 and 293.5 m^2 g^{-1}, respectively, in B-700 (Table 1). Previous investigations on *Miscanthus* biochar reported that SSA of micropores ranged from 2.4 to 381.5 m^2 g^{-1}, and sharply increased in PT range between 400 and 600 °C [56]. Luo et al. [57] and Han et al. [17] ascribed this SSA increase to progressive volatilization of cellulose, hemicellulose and lignin as temperature increased, since volatilization causes formation of channel structures with larger pore-size, increasing total SSA. The percentage of particles having a given equivalent diameter (<25 μm, 25-53 μm and 53-106 μm) was 14.7, 52.8 and 32.5% for B-400, and 5.6, 62.0 and 22.4% for B-700, respectively.

Numerous studies on biochar have related some molar elemental rations such as (O+N)/C, H/C and O/C to polarization, carbonization and hydrophilization, respectively [58,59]. In this study, B-400 had a (O+N)/C of 0.37, O/C of 0.36 and H/C of 0.05, whereas B-700 had 0.25, 0.24 and 0.01, respectively, due to increased C and decreased H, N, O and S contents [60], indicating decreased polarization and hydrophilization and increased carbonization with increasing PT. Previous studies have shown that *Miscanthus* biochar produced at 400 °C had a (O+N)/C ranging between 0.26 and 0.48, O/C between 0.26 and 0.48, and H/C between 0.05 and 0.09, while those produced at 700 °C had the respective ratios ranged from 0.08 to 0.09, 0.07 to 0.08, and was 0.02 [16,61]. The yield and ash content of biochar were 31.0 and 8.8 for B-400, and

Table 1. Physicochemical characteristics of *Miscanthus* biochar produced at two pyrolysis temperatures at 400 °C (B-400) and 700 °C (B-700)

Biochar	Specific surface area (m^2 g^{-1})		Elemental composition (%)					Atomic ratio			Acidic functional group (mmol g^{-1})				PZNC[a]	Yield (%)	Ash (%)
	Micro-pores	Nano-pores	C	H	O	N	S	(O+N)/C	H/C	O/C	Carboxylic	Lactonic	Phenolic	Total			
B-400	5.6	191.6	70.5	3.5	25.3	0.6	0.02	0.37	0.05	0.36	0.150	0.167	0.421	0.74	8.8	31.0	8.8
B-700	236.3	293.5	79.2	1.1	19.2	0.4	0.02	0.25	0.01	0.24	0.013	0.125	0.013	0.15	10.0	26.0	11.6

[a]PZNC denotes the point-of-zero net charge

26.0 and 11.6 for B-700, respectively.

The PZNC was determined as 8.8 for B-400 and 10.0 for B-700, thus indicating that more alkalines, metal oxides and minerals were released from the latter, causing the development of more positively charged sites at a given pH [62]. Since solution-pH determines its net surface charge, biochar can have positively and negatively charged surfaces for hydrophilic interactions at a given pH [63]. This means that net surface charge of B-400 and B-700 is positive at circumneutral pH, with more positive charges at the surface of the latter. The acidity of B-400 and B-700 was measured at 0.150 and 0.013 mmol g^{-1} for carboxylic acid groups, 0.167 and 0.125 mmol g^{-1} for lactonic acid groups, and 0.421 and 0.013 mmol g^{-1} for phenolic acid groups, respectively, and the decrease in the acidity of surface functional groups with increasing PT was due to volatilization of oxygen-containing structures [15,64]. The XRF results of B-400 and B-700 revealed that each concentration of Si, K, Ca, P, Mg, S, Al and Fe was below 1%. Concentrations of Si were 0.60% for biochar feedstock, 1.61% for B-400 and 2.35% for B-700, as a result of Si-accumulation due to pyrolysis (Table S1).

2. Structural Transformation of Biochar

Compared with biochar feedstock, the bands representing vibrations for polysaccharide, aliphatic, ester, phenol and carbohydrate structures disappeared during pyrolysis, while those indicating double bonds of aromatic C=C (1,596 cm^{-1}) and carbonyl C=O (1,695 cm^{-1}) [10] appeared in B-400, but completely disappeared in B-700 (Fig. 1), leaving only lignin C=C (1,540 cm^{-1}) and Si-containing structures (1,200-900 cm^{-1}). Relative intensities of biochar peaks were lower at higher PT (700 °C) due to the formation of ring-structured lignin C=C and concomitant decreases in carbonyl C=O and aromatic C=C (Fig. 1), creating larger pores (Table 1). This was corroborated by the scanning electron photomicrograph (SEM) images (Fig. S1). We therefore observed the decrease in the acidity of surface functional group with increasing PT and the related structural transformation to aromatic structures (Table 1).

In both biochars, the band indicating Si-O-Si and Si-O vibrations appeared at 1,094 cm^{-1} [21]. The XRF spectrograms of biochar also corroborated Si-accumulation and mineral deposits (Table S1). Xiao et al. [65] reported an accumulation of Si-containing structures and a concurrent decrease in single bonds among C, S and O atoms in biochar with increasing PT. Therefore, we inferred that pyrolysis caused conversion of single-bond structures of *Miscanthus* feedstock into aromatic structures with Si-accumulation. Further pyrolysis to 700 °C led to the formation of ligneous structures with mineral salt deposits, increasing SSA due to the increase in micro-pore (larger pore) volumes (Fig. 1 and Table 1).

Apparent density of biochar increases with increasing activation during pyrolysis due to the collapse of pores [66], and was 0.43 Mg m^{-3} for B-400 and 0.48 Mg m^{-3} for B-700. The SEM photomicrographs (Fig. S1) and XRF spectrograms (Table S1) supported the accumulation of mineral salts on biochar surface, suggesting a probable contribution of mineral surface moieties of biochar to simazine sorption. However, since sorption distribution coefficients (K_d) for triazine onto mineral surfaces in the literature were very low [67] and the mineral fractions of our *Miscanthus* biochar were low (3.0% for B-400 and 4.3% for B-700) (Table S1), we disregarded the contribution of mineral surfaces of biochar to the sorption of simazine.

3. Sorption Kinetics, Speciation, and Degradation

Although sorption equilibrium was reached within 24 h for both biochar (Fig. S2), we conducted all batch experiments for 81 h to guarantee the achievement of equilibrium under various experimental conditions. The mole ratio of neutral to protonated simazine species was 0.60 at pH 1.9, and increased to near unity at pH 5; this increasing pattern fitted well to theoretical calculation using the Henderson-Hasselbalch equation (Fig. 2). Rates of simazine degradation (k_{dg}) were 0.012 at pH 1.0 and 0.032 h^{-1} at pH 12.1, while its degradation did not occur across the two pH extremes (2.0≤pH≤10.0) (Fig. 2). Therefore, we disregarded degradation and protonation of simazine across working pH ranges (3.5≤pH≤10).

Simazine degrades abiotically through chemical and photolytic processes [68]; however, the possibility of photodegradation was

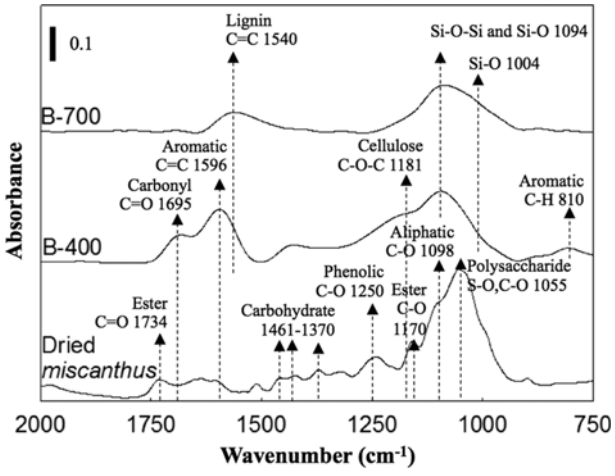

Fig. 1. Stacked ATR FT-IR spectra of dried *Miscanthus* and biochar produced at 400 °C (B-400) and 700 °C (B-700). Arrows and numbers indicate the frequency of the vibration mode in the molecular structure.

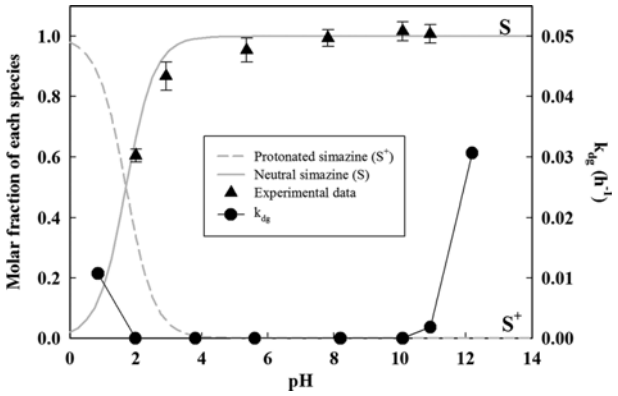

Fig. 2. Molar fraction of protonated (gray dashed line) and neutral (gray solid line) simazine calculated using the Henderson-Hasselbach equation and of neutral simazine obtained from batch experiments (solid triangle) as a function of solution pH and the first-order degradation kinetics (k_{dg}) of simazine estimated by varying the pH (solid circle with a line).

disregarded by encapsulation of simazine samples with airtight amber vials. Simazine remains stable in neutral pH range, but becomes unstable under extremely acidic or alkaline conditions. Simazine has been known to undergo hydrolytic dechlorination due to protonation of lone-pair electrons on the N atom in the aromatic ring structure and subsequent cleavage of C-Cl bond due to electron deficiency under acidic conditions and to the direct nucleophilic substitution of Cl by OH under alkaline conditions [69,70].

4. Sorption Isotherm

Equilibrium sorption data were fitted to the Langmuir and Freundlich isotherms to identify the sorption mechanisms of simazine onto biochar, and to the Dubinin-Radushkevich isotherm to estimate E_s. Fitted isotherm parameters indicated that simazine sorption data obtained at three set pH values of 3, 6 and 9 fitted best to the Freundlich model (Fig. 3) in terms of average R^2 and Δq (Table 2). In this pH region, simazine molecule remains undegraded, while surface acidity of biochar changes at pH 4-5 due to its carboxylic acid groups and at pH 7-8 due to its lactonic acid groups [29].

From the Dubinin-Radushkevich isotherm plots, the isotherm constant β was calculated as 0.1021 for B-400 and 0.1392 for B-700; the maximum sorption capacity (q_{max}) was 1,154.5 and 856.9 mg kg^{-1}, respectively. The corresponding mean free energy (E_s) was calculated as 1.72-2.92 kJ mol^{-1} for B-400 and 1.46-2.54 kJ mol^{-1} for B-700, thus indicating that the sorption of simazine to biochar followed physisorption. Relatively high values of E_s indicate enthalpy-related sorption, while relatively low values indicate entropy-related sorption [39]. If E_s lies between 0-8 kJ mol^{-1}, the sorption process follows physisorption, while a value of E_s between 8-16 kJ mol^{-1} indicates chemisorption [71]. In general, q_{max} and E_s decreased with increasing pH and PT, while the isotherm constant increased (Table 2). Based on the results, we infer that the sorption of simazine occurs at heterogeneous sorption sites of biochar surface with a non-uniform distribution of sorption energy, and this inference was well predicted by the results of previous studies [18,40].

Decrease in K_F (a proxy of sorption capacity) of the Freundlich model from 1,104 to 546 for B-400 and from 643 to 427 in B-700 with increasing pH (Table 2) indicated that the sorption capacity

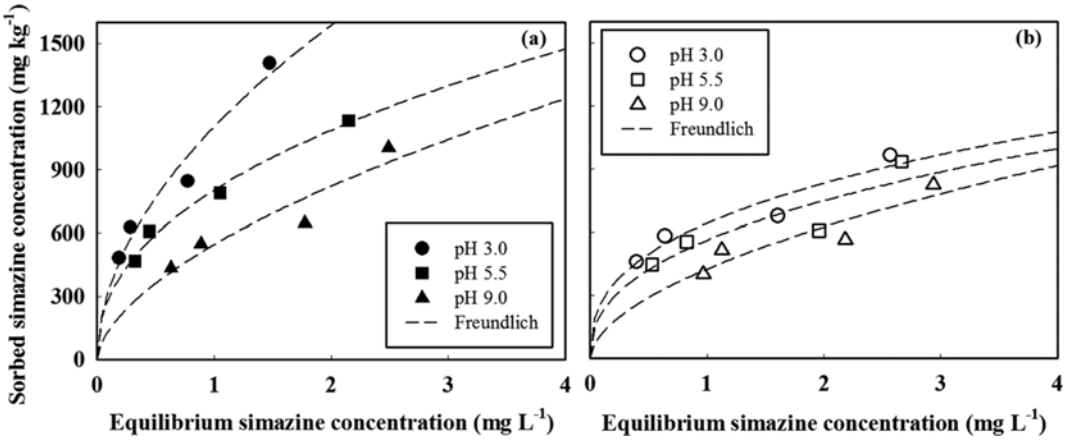

Fig. 3. Fitting of the Freundlich isotherm to each dataset of simazine sorption obtained at three set pH values [3.0 (circle), 5.5 (rectangle) and 9 (triangle)] for (a) B-400 and (b) B-700.

Table 2. Isotherm parameters for sorption of simazine on the *Miscanthus* biochar produced pyrolysis temperatures at 400 °C (B-400) and 700 °C (B-700). The biochar dosage was 2.5, 5.0, 7.5 and 10 g L^{-1} with 5 mg L^{-1} simazine at pH 3.0, 5.5 and 9.0, and the mixture was agitated at 160 rpm for 81 h at 25 °C. The value in parentheses indicates the standard error of the fitted result

Biochar	pH	Langmuir isotherm				Freundlich isotherm				Dubinin-Radushkevich isotherm				
		K_L	q_{max}	R^2	Δq	K_F	1/n	R^2	Δq	β	q_{max}	E_s	R^2	Δq
B-400	3.0	1.44	1939	0.90	16.3	1104	0.523	0.96	10.3	0.059	1361	2.92	0.83	18.7
	(0.02)	(0.85)	(520)			(63.0)	(0.09)			(0.02)	(212)			
	5.5	1.43	1452	0.96	7.42	803.3	0.438	0.99	5.35	0.079	1122	2.52	0.91	10.3
	(0.26)	(0.41)	(170)			(21.3)	(0.04)			(0.02)	(105)			
	9.0	0.50	1665	0.85	14.5	546.2	0.590	0.88	12.5	0.169	980.5	1.72	0.76	16.8
	(0.03)	(0.41)	(733)			(62.8)	(0.16)			(0.07)	(161)			
B-700	3.0	1.67	1089	0.85	11.7	643.0	0.372	0.91	9.10	0.078	894.8	2.54	0.78	13.3
	(0.02)	(0.89)	(194)			(41.9)	(0.09)			(0.03)	(108)			
	5.5	1.21	1078	0.73	16.3	563.1	0.412	0.79	14.6	0.105	844.8	2.18	0.66	17.4
	(0.57)	(0.96)	(312)			(69.2)	(0.16)			(0.06)	(136)			
	9.0	0.47	1315	0.81	13.3	426.8	0.551	0.84	12.4	0.235	831.0	1.46	0.75	14.5
	(0.21)	(0.37)	(540)			(61.2)	(0.17)			(0.10)	(127)			

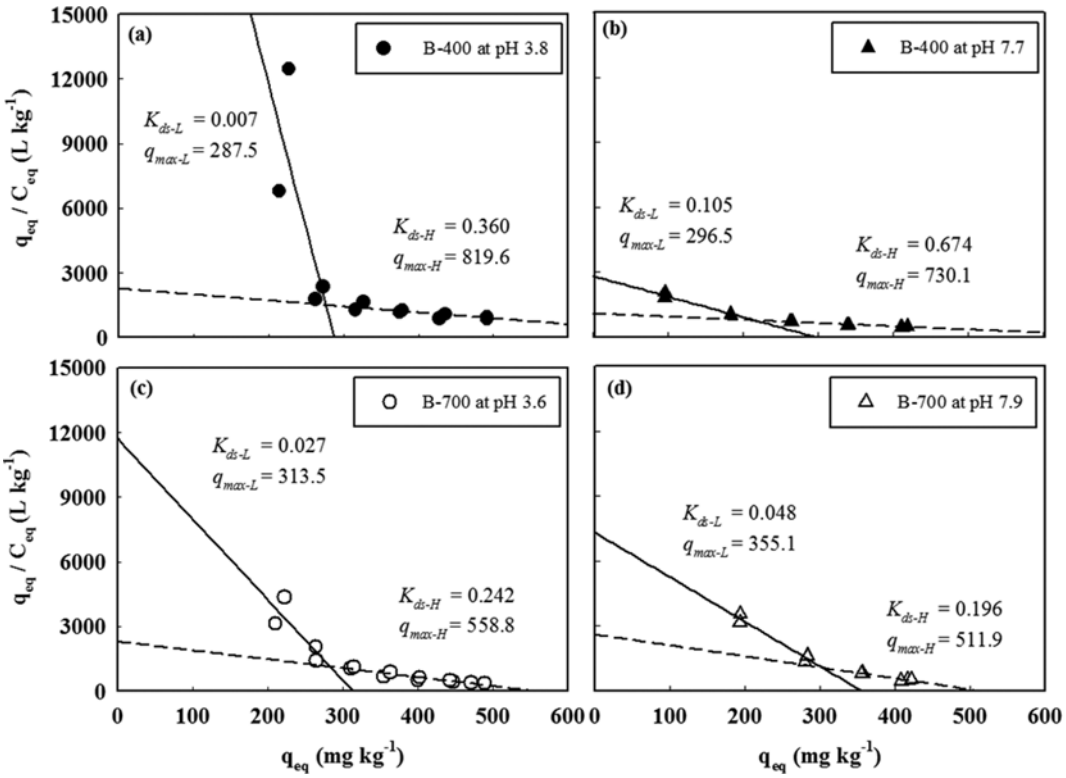

Fig. 4. Scatchard plot (y-axis: the ratio of biochar-bound simazine to free simazine, q_{eq}/C_{eq}; x-axis: q_{eq}) showing two types of sorption mechanism between simazine and biochar obtained at: (a) pH=3.8 (solid circle) and (b) pH=7.7 (solid triangle) for B-400, and (c) pH=3.6 (open circle) and (d) pH=7.9 (open triangle) for B-700. Data points represent experimental results. Solid lines represent electrostatic interaction; dashed lines denote hydrophobic interaction.

of biochar would vary with pH, posing a challenge to our presumption that hydrophobic interactions would be a dominant process for simazine sorption to biochar surface. To date, few attempts have been made to predict the pH-dependent sorption-behavior of organic pollutants on biochar surface. Yang et al. [35] reported that the maximum sorption of diuron occurred at pH 2.5, while ametryne showed its maximum sorption at pH 4.0. Zheng et al. [40] demonstrated that simazine sorption gradually decreased with increasing pH. Jia et al. [25] observed that K_F of oxytetracycline sorption to maize-straw-derived biochar varied with solution-pH. Previous investigations on the sorption of organic pollutants with ionizable functional groups suggested that their sorption capacity decreases with increasing pH due to electrostatic repulsion between ionizable organic pollutants and biochar [72,73]. In our study, however, neutral simazine remained undegraded over a wide pH range from 3 to 10 (Fig. 2).

Contrary to our presumption that the sorption capacity of biochar would increase due to an increase in SSA [61,74], our results clearly show that the mean value of the parameters related to sorption capacity (K_F and q_{max}) of biochar decreased with increasing PTs (Table 2), while SSA increased (Table 1). In particular, the values of K_F and q_{max} also decreased (Table 2) as more pH-dependent sorption sites were deprotonated with increasing pH and PT [75], resulting in decreased sorption of neutral simazine (Fig. 3).

5. Scatchard Plot Analysis of Simazine Sorption

Estimates of the fitted values of E_s (Table 2) indicated simazine sorption followed an entropy-related physisorption. Concave-upward Scatchard plots indicated the presence of two classes of binding sites with differing K_{ds} and/or involvement of at least two sorption processes (Fig. 4). Nonlinear Scatchard plots indicate involvement of more than one sorption process [55]. The nonlinearity may imply the presence of two types of binding sites having different affinities for the simazine sorption. Therefore, we calculated K_{ds} and q_{max} for two sorption sites: the lower sorption-range (type-L) and the higher sorption-range (type-H). The suffixes after K_{ds} and q_{max} indicate the lower and higher sorption-ranges.

Increasing pH increased K_{ds-L} from 0.007 to 0.105 mg L^{-1} and q_{max-L} from 287.5 to 296.5 mg kg^{-1} for B-400, and from 0.027 to 0.048 mg L^{-1} and from 313.5 to 355.1 mg kg^{-1} for B-700. However, K_{ds-H} increased in B-400 but decreased in B-700, while q_{max-H} decreased (Fig. 4). In contrast, increasing PT decreased K_{ds-H} from 0.242 to 0.196 mg L^{-1} and q_{max-H} from 558.8 to 511.9 mg kg^{-1}; however, K_{ds-L} responded oppositely to pH, while q_{max-L} increased (Fig. 4).

From these relationships, we infer that pH affected simazine sorption more in the lower sorption-range, while sorption affinity of biochar decreased as pH increased. In contrast, PT affected more in the higher sorption-range, lowering q_{max} and raising sorption affinity of biochar at higher PT. Therefore, we deduced that K_{ds-L} responded sensitively to pH in the lower sorption-range, which causes change in the electrostatic field, while K_{ds-H} was responsible for simazine sorption associated with changes in surface and pore-structure modification caused by PT changes (Table 1) in the higher

sorption-range. Therefore, increases in pH decreased $K_{ds\text{-}L}$ more in B-400 than in B-700 (Table 1), while increases in PT decreased $K_{ds\text{-}H}$ more at higher pH than at lower pH. Estimates of the fitted K_{ds} and q_{max} indicated that the maximum sorption (the sum of $q_{max\text{-}L}$ and $q_{max\text{-}H}$) of simazine decreased as pH and/or PT increased (Fig. 3).

Three possible binding mechanisms are involved in the sorption of simazine onto biochar surface: van der Waals (vdW) forces, π-π electron donor-acceptor (EDA) interactions, and weak H-bonding [76]. Based on the Scatchard plot analysis, we could ascribe strong electrostatic attraction (S_{es}) to a dominant sorption mechanism in the lower sorption-range [77], and a relatively weak hydrophobic attraction (S_{hp}) to another process that governs in the higher sorption-range [78], since the EDA or H-bonding interactions are responsible for S_{es} and the vdW interactions explain S_{hp} [79,80]. As a result, we found that two types of binding sites of biochar responded independently to changing pH and/or PT.

6. Sorption Mechanism

Based on the physicochemical characteristics of biochar and batch sorption results, we addressed two questions about simazine sorption in response to changes in pH and PT. The first question is the causal relationships for decrease q_{max} with increasing pH (Fig. 4). At pH 3.6 or 3.8 (almost pK_a+2), simazine behaves as a neutral molecule, causing strong S_{hp} with positively charged biochar while weakening the contribution of S_{es}. Increase in pH to 7.7 or 7.9 induces deprotonation of acidic carboxylic groups, decreasing sorption affinity of biochar to neutral simazine due to increased negative charge densities on biochar surface, which therefore decreases q_{max} due to increased electrostatic and/or hydrophobic repulsion [58]. However, despite increased $K_{ds\text{-}L}$, $q_{max\text{-}L}$ slightly increased, indicating the presence of attractive electrostatic interactions as surface negativity increased [81]. This phenomenon was corroborated by the experimental sorption data that were fitted to the Freundlich model (Fig. 3). Therefore, we concluded that pH is a major factor that governs simazine sorption through S_{es} that controls deprotonation of acidic functional groups of biochar and protonation of simazine.

Second, we observed that q_{max} decreased with increasing PT (Table 2), while SSA increased (Table 1). This observation is not consistent with previous results that the sorption of organic pollutants to biochar increased as SSA increased [58,59]. In this study, we found that SSA increased with pore-size enlargement due to pore-structure deformation during pyrolysis as PT increased (Table 1). Increase in PT induced deformation of smaller pores to more open-structured larger pores that may provide more accessible sorption sites (Table 1), leading to increased biochar sorption affinity at a given pH. However, increases in PT decreased maximum sorption over a higher sorption-range ($q_{max\text{-}H}$), while the affinity of biochar for simazine increased, indicating possible unstable simazine sorption favoring desorption in large micro-pores prior to sorption-desorption equilibrium. Lian et al. [82] observed that during the sorption/desorption process, desorption of organic pollutants was less hindered in relatively smaller nanopores with turbostratic and partly compartmentalized structures. However, simazine sorption to biochar in lower sorption-range ($q_{max\text{-}L}$) increased with PT (Fig. 4), and this increase was due to S_{es} [82]. However, PT-induced deformation of pore-structure resulted in overall decrease in q_{max}, and this deduction agrees well with experimental sorption data (Fig. 3). Therefore, we also concluded that PT is a dominant factor that governs simazine sorption through S_{hp} due to deformation of smaller pores to open-structured pores.

CONCLUSIONS

We hypothesized that pH would determine the surface charge density of biochar and simazine that alters the response of simazine sorption, and this response would vary with PT. Pyrolysis resulted in conversion of single bond structures of *Miscanthus* feedstock into aromatic structures with Si-accumulation, and further pyrolysis at 700 °C led to the formation of ligneous structures with mineral salt deposits and increased SSA due to an increase in micropore. Alterations in pore-structures and surface-minerals of biochar with concave-upward Scatchard plots corroborated the existence of at least two dominant sorption mechanisms with multiple types of binding sites: strong sorption process due to electrostatic attraction and weak sorption process *via* hydrophobic attraction. Overall, q_{max} decreased as pH and PT increased. Decreases in $q_{max\text{-}L}$ with increasing pH could be explained by decreases in S_{es} due to progressive deprotonation of acidic functional groups, decreasing positively charged surface of biochar. However, decrease in $q_{max\text{-}H}$ with increasing PT was due to decrease in S_{hp}, resulting from progressive deformation of pore-structure. The results confirmed our hypothesis that solution-pH and PT differently affect the sorption of simazine containing lone-pair electrons onto the surface of biochar with variable surface charge density. We believe that our approach and findings would contribute to a more comprehensive understanding of the sorption mechanisms of ionizable organic pollutants (sorbate) to the surface of biochar (variable-charge sorbent) that would help better interpret their transport and fate under natural soil conditions.

ACKNOWLEDGEMENTS

This research was supported by the Basic Science Research Program through the National Research Foundation of Korea (NRF) (NRF-2016R1D1A1B03934038 and NRF-2014R1AA1A2059196) and by the Brain Korea 21 PLUS program, funded by the Ministry of Education of Korea. We are grateful to Professor Seunghun Hyun and his research team for supplying Miscanthus biochar samples.

SUPPORTING INFORMATION

Additional information as noted in the text. This information is available via the Internet at http://www.springer.com/chemistry/journal/11814.

REFERENCES

1. J. Lehmann, *Nature*, **447**, 143 (2007).
2. C. J. Atkinson, J. D. Fitzgerald and N. A. Hipps, *Plant Soil.*, **337**, 1 (2010).
3. L. Van Zwieten, S. Kimber, S. Morris, K. Y. Chan, A. Downie, J. Rust, S. Joseph and A. Cowie, *Plant Soil.*, **327**, 235 (2010).

4. F. Li, K. Shen, X. Long, J. Wen, X. Xie, X. Zeng, Y. Liang, Y. Wei, Z. Lin, W. Huang and R. Zhong, *PLoS One*, **11**, 7 (2016).
5. S. Kloss, F. Zehetner, E. Oburger, J. Buecker, B. Kitzler, W. W. Wenzel, B. Wimmer and G. Soja, *Sci. Total Environ.*, **481**, 498 (2014).
6. G. Xu, Y. Zhang, J. Sun and H. Shao, *Sci. Total Environ.*, **568**, 910 (2016).
7. S. Kloss, F. Zehetner, A. Dellantonio, R. Hamid, F. Ottner, V. Liedtke, M. Schwanninger, M. H. Gerzabek and G. Soja, *J. Environ. Qual.*, **41**, 990 (2012).
8. L. Zhao, X. Cao, O. Mašek and A. Zimmerman, *J. Hazard. Mater.*, **256-257**, 1 (2013).
9. A. Mukherjee, A. R. Zimmerman and W. Harris, *Geoderma.*, **163**, 247 (2011).
10. B. Chen, D. Zhou and L. Zhu, *Environ. Sci. Technol.*, **42**, 5137 (2008).
11. T. Mimmo, P. Panzacchi, M. Baratieri, C. A. Davies and G. Tonon, *Biomass Bioenergy*, **62**, 149 (2014).
12. D. H. Lee and D. T. Liang, *Energy Fuels*, **20**, 388 (2006).
13. J. Lehmann, *Front. Ecol. Environ.*, **5**, 381 (2007).
14. G. Zhang, Q. Zhang, K. Sun, X. Liu, W. Zheng and Y. Zhao, *Environ. Pollut.*, **159**, 2594 (2011).
15. W. Song and M. Guo, *J. Anal. Appl. Pyrolysis.*, **94**, 138 (2012).
16. A. Budai, L. Wang, M. Gronli, L. T. Strand, M. J. Antal, S. Abiven, A. Dieguez-alonso, A. Anca-couce and D. P. Rasse, *J. Agric. Food Chem.*, **62**, 3791 (2014).
17. L. Han, L. Qian, J. Yan and M. Chen, *Chemosphere*, **156**, 262 (2016).
18. X. Cao, L. Ma, B. Gao and W. Harris, *Environ. Sci. Technol.*, **43**, 3285 (2009).
19. L. Qian and B. Chen, *Environ. Sci. Technol.*, **47**, 8759 (2013).
20. M. Uchimiya, S. Chang and K. T. Klasson, *J. Hazard. Mater.*, **190**, 432 (2011).
21. Y. Xu and B. Chen, *J. Soils Sediments*, **15**, 60 (2015).
22. P. Oleszczuk, S. E. Hale, J. Lehmann and G. Cornelissen, *Bioresour. Technol.*, **111**, 84 (2012).
23. M. Ahmad, S. S. Lee, X. Dou, D. Mohan, J. K. Sung, J. E. Yang and Y. S. Ok, *Bioresour. Technol.*, **118**, 536 (2012).
24. L. Zhao, X. Cao, W. Zheng, Q. Wang and F. Yang, *Chemosphere*, **136**, 133 (2015).
25. M. Jia, F. Wang, Y. Bian, X. Jin, Y. Song, F. O. Kengara, R. Xu and X. Jiang, *Bioresour. Technol.*, **136**, 87 (2013).
26. M. Uchimiya, I. M. Lima, K. Thomas Klasson, S. Chang, L. H. Wartelle and J. E. Rodgers, *J. Agric. Food Chem.*, **58**, 5538 (2010).
27. J. Wang, F. Wang, J. Yao, H. Guo, R. E. Blake, M. M. F. Choi and C. Song, *Anal. Lett.*, **46**, 379 (2013).
28. Q. Fang, B. Chen, Y. Lin and Y. Guan, *Environ. Sci. Technol.*, **48**, 279 (2014).
29. C. Leon and L. R. Radovic, *Abstr. Pap. Am. Chem. Soc.*, **202**, 1007 (1991).
30. C. Flores, V. Morgante, M. González, R. Navia and M. Seeger, *Chemosphere*, **74**, 1544 (2009).
31. M. Silva and P. Iyer, *Birth Defects Res. B. Dev. Reprod. Toxicol.*, **101**, 308 (2014).
32. D. M. Whitacre, *Rev. Environ. Contam. Toxical.*, **202**, 1 (2010).
33. R. Celis, J. Cornejo, M. C. Hermosín and W. C. Koskinen, *Soil Sci. Soc. Am. J.*, **61**, 436 (1997).
34. J. B. Weber, *Soil Sci. Soc. Am. J.*, **34**, 401 (1970).
35. Y. Yang, Y. Chun, G. Sheng and M. Huang, *Langmuir*, **20**, 6736 (2004).
36. A. R. Betts, N. Chen, J. G. Hamilton and D. Peak, *Environ. Sci. Technol.*, **47**, 14350 (2013).
37. S. Fang, D. C. W. Tsang, F. Zhou, W. Zhang and R. Qiu, *Chemosphere*, **149**, 263 (2016).
38. D. T. Grubb, *J. Mater. Sci.*, **9**, 1715 (1974).
39. H. Liu and W. Chen, *RSC Adv.*, **5**, 27034 (2015).
40. W. Zheng, M. Guo, T. Chow, D. N. Bennett and N. Rajagopalan, *J. Hazard. Mater.*, **181**, 121 (2010).
41. G. Sigmund, T. Hüffer, T. Hofmann and M. Kah, *Sci. Total Environ.*, **580**, 770 (2017).
42. H. P. Boehm, *Carbon N. Y.*, **32**, 759 (1994).
43. R. B. Fidel, D. A. Laird and M. L. Thompson, *J. Environ. Qual.*, **42**, 1771 (2013).
44. A. Contescu, C. Contescu, K. Putyera and J. A. Schwarz, *Carbon N. Y.*, **35**, 83 (1997).
45. X. Cao and W. Harris, *Bioresour. Technol.*, **101**, 5222 (2010).
46. M. Stefaniuk and P. Oleszczuk, *J. Anal. Appl. Pyrolysis.*, **115**, 157 (2015).
47. A. S. Gunasekara, J. Troiano, K. S. Goh and R. S. Tjeerdema, *Rev. Environ. Contam. Toxicol.*, **189**, 1 (2007).
48. V. Morgante, C. Flores, X. Fadic, M. González, M. Hernández, F. Cereceda-Balic and M. Seeger, *J. Environ. Manage.*, **95**, S300 (2012).
49. P. A. Bersanetti, R. M. R. G. Almeida, M. Barboza, M. L. G. C. Araújo and C. O. Hokka, *Biochem. Eng. J.*, **23**, 31 (2005).
50. K. Foo and B. Hameed, *Pet. Coal.*, **56**, 552 (2014).
51. A. Da¸browski, *Adv. Colloid Interface Sci.*, **93**, 135 (2001).
52. L. Mihaly Cozmuta, A. Mihaly Cozmuta, A. Peter, C. Nicula, E. Bakatula Nsimba and H. Tutu, *Water SA.*, **38**, 269 (2012).
53. E. Pehlivan, B. H. Yanik, G. Ahmetli and M. Pehlivan, *Bioresour. Technol.*, **99**, 3520 (2008).
54. O. Gezici, H. Kara, M. Ersöz and Y. Abali, *J. Colloid Interface Sci.*, **292**, 381 (2005).
55. O. Gezici, H. Kara, S. Yanik, H. F. Ayyildiz and S. Kucukkolbasi, *Colloids Surf., A.*, **298**, 129 (2007).
56. W. K. Kim, T. Shim, Y. S. Kim, S. Hyun, C. Ryu, Y. K. Park and J. Jung, *Bioresour. Technol.*, **138**, 266 (2013).
57. L. Luo, C. Xu, Z. Chen and S. Zhang, *Bioresour. Technol.*, **192**, 83 (2015).
58. B. Chen and Z. Chen, *Chemosphere*, **76**, 127 (2009).
59. Z. Chen, B. Chen and C. T. Chiou, *Environ. Sci. Technol.*, **46**, 11104 (2012).
60. M. Keiluweit, P. S. Nico, M. Johnson and M. Kleber, *Environ. Sci. Technol.*, **44**, 1247 (2010).
61. P. A. Trazzi, J. J. Leahy, M. H. B. Hayes and W. Kwapinski, *J. Environ. Chem. Eng.*, **4**, 37 (2016).
62. M. I. Al-Wabel, A. Al-Omran, A. H. El-Naggar, M. Nadeem and A. R. A. Usman, *Bioresour. Technol.*, **131**, 374 (2013).
63. A. Silber, Levkovitch and E. R. Graber, *Environ. Sci. Technol.*, **44**, 9318 (2010).
64. Y. Chun, G. Sheng, G. T. Chiou and B. Xing, *Environ. Sci. Technol.*, **38**, 4649 (2004).
65. X. Xiao, B. Chen and L. Zhu, *Environ. Sci. Technol.*, **48**, 3411 (2014).
66. W. Ding, X. Dong, I. M. Ime, B. Gao and L. Q. Ma, *Chemosphere*, **105**, 68 (2014).
67. L. Clausen, I. Fabricius and L. Madsen, *J. Environ. Qual.*, **30**, 846

(2001).
68. A. Rahman and P. T. Holland, *New Zeal. J. Exp. Agric.*, **13**, 59 (1985).
69. D. E. Armstrong, G. Chesters and R. F. Harris, *Soil Sci. Soc. Am. J.*, **31**, 61 (1967).
70. N. Burkhard and J. A Guth, *Pestic. Sci.*, **12**, 45 (1981).
71. M. S. Samuel, M. E. A. Abigail and C. Ramalingam, *PLOS ONE*, **10**, 1 (2015).
72. A. U. Rajapaksha, M. Vithanage, M. Ahmad, D. C. Seo, J. S. Cho, S. E. Lee, S. S. Lee and Y. S. Ok, *J. Hazard. Mater.*, **290**, 43 (2015).
73. L. P. Lingamdinne, H. Roh, Y. L. Choi, J. R. Koduru, J. K. Yang and Y. Y. Chang, *J. Ind. Eng. Chem.*, **32**, 178 (2015).
74. Z. Chen, B. Chen, D. Zhou and W. Chen, *Environ. Sci. Technol.*, **46**, 12476 (2012).
75. L. Ping, Y. Zhuoxin, L. Jianfeng, J. Qiang, D. Yaofang, F. Qiaohui and W. Wangsuo, *Environ. Sci. Process. Impacts*, **16**, 2278 (2014).
76. D. Zhu, S. Hyun, J. J. Pignatello and L. S. Lee, *Environ. Sci. Technol.*, **38**, 4361 (2004).
77. C. M. Park, J. Han, K. H. Chu, Y. A. J. Al-Hamadani, N. Her, J. Heo and Y. Yoon, *J. Ind. Eng. Chem.*, **48**, 186 (2017).
78. Z. Xu, D. Kuang, L. Liu and Q. Deng, *J. Pharm. Biomed. Anal.*, **45**, 54 (2007).
79. A. A. Krichko and S. G. Gagarin, *Fuel*, **69**, 885 (1990).
80. T. D. Gauthier, W. R. Seitz and C. L. Grant, *Environ. Sci. Technol.*, **21**, 243 (1987).
81. Y. Qiu, Z. Zheng, Z. Zhou and G. D. Sheng, *Bioresour. Technol.*, **100**, 5348 (2009).
82. F. Lian, F. Huang, W. Chen, B. Xing and L. Zhu, *Environ. Pollut.*, **159**, 850 (2011).